Published in final edited form as:
Acc Chem Res. 2011 October 18; 44(10): 936–946. doi:10.1021/ar200023x.

Theranostic Nanoshells: From Probe Design to Imaging and Treatment of Cancer

Rizia Bardhan[†,‡], **Surbhi Lal**[⊥], **Amit Joshi**[§], and **Naomi J. Halas**[†,⊥,∥,*]

[†]Department of Chemistry, Rice University, Houston, TX 77005

[⊥]Department of Electrical and Computer Engineering, Rice University, Houston, TX 77005

[∥]Department of Bioengineering, Rice University, Houston, TX 77005

[§]Department of Radiology, Baylor College of Medicine, Houston, TX 77030

CONSPECTUS

Recent advances in theranostics have expanded our ability to design and construct multifunctional nanoparticles that will ultimately allow us to image and treat diseases in a single clinical procedure. Theranostic nanoparticles, combining targeting, therapeutic and diagnostic functions within a single nanoscale complex, have emerged as a result of this confluence of nanoscience and biomedicine. The theranostic capabilities of gold nanoshells -spherical, silica core, gold shell nanoparticles- have attracted tremendous attention over the past decade as nanoshells have emerged as a promising tool for cancer therapy and bioimaging enhancement. This account examines the design and synthesis of nanoshell-based theranostic agents, their plasmon-derived optical properties and their corresponding applications. Nanoshells illuminated with resonant light are either strong optical absorbers or scatterers, properties which give rise to their unique capabilities. In this account, we discuss the underlying physical principles contributing to the photothermal response of nanoshells. We elucidate the photophysics of nanoshell-induced fluorescence enhancement of weak near-infrared fluorophores. We then describe the application of nanoshells as a contrast agent for optical coherence tomography of breast carcinoma cells *in vivo*. We also examine the recent progress of nanoshells as a multimodal theranostic probe for near-infrared fluorescence and magnetic resonance imaging (MRI) combined with photothermal ablation of cancer cells. The design and preparation of nanoshell complexes is discussed, and their ability to enhance the photoluminescence of fluorophores while incorporating MR contrast is described. We show the theranostic potential of the multimodal nanoshells *in vivo* for imaging subcutaneous breast cancer tumors in animal models and their biodistribution in various tissues.

We then discuss the potential of nanoshells as light-triggered gene therapy vectors. The plasmonic properties of nanoshells make them highly effective as light controlled delivery vectors, adding temporal control to the spatial control characteristic of nanoparticle-based gene therapy approaches. We describe the fabrication of DNA-conjugated nanoshell complexes and compare the efficiency of light-induced and thermally-induced DNA release of DNA. We examine light-triggered release of DAPI (4',6-diamidino-2-phenylindole) molecules, which bind reversibly to double-stranded DNA, to visualize intracellular light-induced release. Finally, we look at future prospects of nanoshell-based theranostics, the potential impact and near-term challenges of theranostic nanomedicine in the next decade.

[*]To whom correspondence should be addressed. halas@rice.edu.
[‡]Current address: Molecular Foundry, Materials Science Division, Lawrence Berkeley National Laboratory, Berkeley, California 94720

Introduction

Despite prodigious advances in our understanding of the disease, cancer remains one of the leading causes of death in the United States. Nearly 1,529,560 new cases of cancer were projected for 2010, with an anticipated mortality rate of 37%.[1] As cancer proliferates, improved diagnostic and therapeutic strategies are imperative for early detection and treatment. The emergence of nanomaterials for potentially transformative advances in biomedicine provides new strategies for combined diagnostics and therapeutics. Conventional diagnostic and therapeutic agents such as chelated Gd^{3+} ions for magnetic resonance imaging (MRI) enhancement,[2] radiolabeled biomolecules, or chemotherapy drugs,[3] are often limited by short blood circulation times and nonspecific biodistribution. Nanoparticle-based complexes have demonstrated extraordinary promise for targeting, imaging and therapeutics at the cellular and molecular level.[4, 5] Nanoparticles provide several potential advantages over conventional agents, including extension of circulating half-life, passive accumulation at tumor sites due to the enhanced permeability and retention (EPR) effect, active targeting of cancer cells, reduced toxicity, and integration of multiple diverse functions in a single complex.[6, 7]

The past two decades have witnessed a rapid increase in the design of nanoparticle-based contrast agents[8] and therapeutic actuators.[9] Recently, these two functionalities have begun to be combined within a single nanoscale complex, resulting in the development of "*theranostic*" nanocomplexes, which are emerging as an alternative to independently administered diagnostic probes and traditional cancer therapy strategies.[10–17] Theranostic probes are a class of agents that can simultaneously deliver diagnostic and therapeutic functions enabling detection and treatment of diseases in a single procedure. Interest in theranostics is rapidly increasing due to the versatility of nanoparticle-based approaches. Since multiple types of molecules can be incorporated onto a single nanoparticle surface, the same nanoscale complex can perform multiple functions. Of particular importance is the combination of targeting species with contrast agents that enable tracking of the theranostic complex.[18, 19] This specific combination of functions can provide valuable biodistribution information, opportunities to study the therapeutic mechanism, and strategies for improving therapeutic efficacy, all *in vivo*. Theranostic nanoparticles can be readily fabricated since the synthetic procedure is typically a combination of well-established chemistries originally developed solely for imaging or therapy. For example, Santra *et al.* combined iron oxide nanoparticles with folate moieties, the near-infrared fluorophore Cy5.5, and the anticancer drug taxol, resulting in a theranostic agent combining targeting (via the folate receptor), dual-modality imaging and chemotherapy.[17] A representative list of theranostic nanoparticles with diverse functionalities is given in Table 1. The demonstration of these multifunctional nanocomplexes and their properties has stimulated a significant increase in the development of combined detection and treatment strategies for cancer.

Gold (Au) based nanostructures have emerged as highly effective platforms for theranostic agents.[20] Like other noble metal nanoparticles, Au nanoparticles (AuNPs) possess vivid optical properties, with strong optical resonances associated with their surface plasmons. Their optical properties are controlled by the geometry and size of the nanoparticle. AuNPs have the additional advantage of biocompatibility, as well as the existence of well known, robust chemistries for binding a range of molecules and functional materials to the AuNP surface. The therapeutic capabilities of Au nanoshells (AuNSs), spherical silica nanoparticles wrapped in a nanoscale Au shell, have been demonstrated extensively.[21] The optical absorption of AuNSs can be tuned to the near-infrared spectral range known as the "water-window" (690 – 900 nm), where tissue is maximally transparent, by varying the relative size of the core and shell.[22] AuNSs resonant in the near-infrared can be strong absorbers or scatterers, depending on particle size, enabling both bioimaging and

photothermal ablation.[23, 24] Tuning the nanoshell resonance to the emission frequency of a weak NIR fluorophore can provide fluorescence enhancement.[25, 26] The bright nanoshell-fluorophore conjugates can be employed for combined fluorescence-based imaging and photothermal ablation.[27–29] The plasmon-based optical properties of AuNSs also enable the efficient release of antisense DNA oligonucleotides conjugated to the complex, providing a light-triggerable, nonviral vector for gene therapy.[30, 31] In our previous review we focused on AuNSs as therapeutic actuators and their corresponding clinical impact.[21] In this review, we emphasize the progress of AuNS-based complexes for theranostic applications which combine fluorescence imaging, MRI and photothermal therapy as well as gene therapy.

Photothermal Properties

Nanoshells were the first nanoparticle used to demonstrate photothermal cancer therapy[32], the transition of this approach to clinical trials is currently underway.[21] The therapeutic response of AuNSs results from their ability to absorb light resonant with the nanoshell plasmon energy and dissipate the light energy thermally. The physical process underlying the photothermal characteristics of noble metal nanoparticles has been studied dynamically.[33] When AuNSs are excited with resonant light, photoexcitation of the electron gas results in rapid nonequilibrium heating. The initial, electronic excitation is followed by subpicosecond relaxation, by means of electron-electron scattering, giving rise to a rapid increase in the surface temperature of the metal. This initial rapid heating is followed by cooling to equilibrium by energy exchange between the electrons and the lattice. At very fast rates of energy dissipation (few picoseconds) relative to lattice cooling, intense photothermal heating can result in the melting or reshaping of the nanostructure, changing its optical characteristics irreversibly.[33] In the first several hundred picoseconds following excitation, the lattice cools via phonons, resulting in heating of the medium directly surrounding the nanostructure. When AuNSs in a cellular medium are illuminated, a large temperature difference between the hot AuNS surface and the cooler surrounding biological medium occurs. This abrupt local temperature increase is responsible for cell death.

Fluorescence Enhancement

When illuminated with resonant light, nanoshell plasmons decay nonradiatively, resulting in absorption, and radiatively, resulting in light scattering. These characteristics can modify the emission properties of fluorophores in their proximity.[25, 26] Fluorescence enhancement or quenching of fluorophores by nearby noble metal surfaces has been known since the pioneering work of Drexhage.[34] The metal-fluorophore interaction results from (i) modification of the electromagnetic field and (ii) the photonic mode density near the fluorophores. For small metal-fluorophore distances (≤ 4 nm), the damping of molecular oscillators by processes such as electron tunneling between the metal and the fluorophore, and image interactions between the two systems, typically lead to strong quenching of the molecular fluorescence. The increase in nonradiative decay rate for short fluorophore-metal distances depends on the inverse cube of the molecule-surface separation.[35] However, for larger metal/fluorophore distances, an increase in the fluorescence intensity can occur, resulting primarily from a combination of enhanced absorption of the fluorophore by the metal's surface field, and an enhanced radiative decay rate of the fluorophore. Both these processes can increase the quantum yield of the fluorophore. At a noble metal nanoparticle (nanoantenna) surface, emission and can be further enhanced by coupling of the fluorescence emission to the far field by scattering.[25] Quantum yield of the near-infrared fluorophore Indocyanine green (ICG), a U.S. Food and Drug Administration (FDA) approved fluorophore, was enhanced from 1% to ~80% by placing them near a AuNS surface. These bright nanoshell-fluorophore conjugates have been used for enhancing sensitivities in fluorescence imaging *in vitro* and *in vivo*.[27, 29]

Optical Imaging and Therapy

The ability of nanoshells to convert absorbed light to heat has been successfully exploited for photothermal therapy.[23, 36] AuNSs designed to scatter light in the NIR physiological "water-window" have also been employed as contrast agents for dark-field scattering,[37] photoacoustic imaging,[38] and optical coherence tomography (OCT).[24] AuNSs of intermediate size (60 nm core radius, 10–12 nm shell thickness) can both absorb and scatter light at 800 nm, and can therefore serve as imaging contrast agents *and* photothermal actuators. AuNSs bound to anti-HER2 antibodies have been demonstrated for dark-field imaging and therapy of SKBR3 breast carcinoma cells.[37] AuNSs have also been examined *in vivo* for enhancement of optical coherence tomography (OCT) and for inducing photothermal cell death.[24] In combining these two functions, it is important to note that the light intensities typically used for imaging are far below those used to induce photothermal effects. For *in vivo* studies, AuNSs were encapsulated with a layer of thiolated-poly(ethylene) glycol (PEG-SH) molecules, where the thiol group is bound to the Au surface. The Poly(ethylene) glycol (PEG) functional group, a non-toxic polymer, is known to reduce nanoparticle aggregation, reduce nonspecific binding *in vivo* and significantly extend blood-circulation time. PEG-conjugated AuNSs were injected intravenously into the tail vein of tumor-bearing mice and allowed to accumulate passively in the tumor. Phosphate buffered saline (PBS) solution was injected in control mice. Twenty hours post-injection, tumors were imaged with a commercial OCT system by placing the imaging probe directly above the tumor, in contact with the skin. Representative OCT images of normal tissue and tumor tissue with both PBS and AuNSs are shown in Figure 1. The enhanced brightness (Fig. 1d) clearly demonstrates that AuNSs provide significant contrast for OCT imaging *in vivo*. Following imaging, tumors were irradiated using a near-infrared laser (808 nm, 4 W/cm^2, 5 mm spot size) for 3 min. Tumor size and animal survival were studied for 7 weeks post treatment. The tumor sizes on the day of treatment and 12 days post-treatment are shown (Fig. 1e). The tumors in all but two mice treated with AuNSs and laser irradiation had completely degenerated in 21 days. The median survival of mice injected with PBS followed by laser treatment was 14 days, and that of the untreated control group was 10 days. Median survival time of AuNS treated mice was longer than 7 weeks, with a long-term survival of 83%.

Multimodal Imaging and Therapy

Nanoshell-based complexes have recently been expanded to include two diagnostic capabilities, MRI and near-infrared fluorescence imaging, in addition to photothermal therapy.[27, 28] Nanocomplexes were constructed by encapsulating AuNSs in a silica epilayer doped with ~10 nm iron oxide (Fe_3O_4) nanoparticles and ICG (Fig. 2a). The nanocomplexes were subsequently functionalized with streptavidin and conjugated with biotinylated antibodies, then passivated with thiolated PEG to reduce nonspecific binding. MR relaxivity, r_2 of the nanocomplexes (Fig. 2b) was observed to be significantly higher than AMI-25 and Resovist, two FDA approved contrast agents in clinical use.[27] Comparison of the fluorescence intensity of the nanocomplexes with an unenhanced ICG solution of equivalent concentration (Fig. 2c), clearly shows the significant enhancement of ICG fluorescence by AuNSs.

The nanocomplexes were tested *in vitro* by targeting human epidermal growth factor receptor (HER2)-expressing breast cancer cells.[27] Nanocomplexes were incubated with HER2-overexpressing SKBR3 cells and HER2 low-expressing MDAMB231 cells as a control, and then imaged using MRI and near-infrared fluorescence. 2D MR images of SKBR3 cells with nanocomplex-antiHER2 conjugates in 0.5% agarose gel (Fig. 3a) reveal hypointense regions, indicating cells labeled with the nanocomplexes. 2D MR images of

nanocomplex–anti-HER2 conjugates incubated with MDAMB231 cells show significantly less MR contrast (Fig. 3b). Intensity projections created by collectively combining all MR image slices show noticeably darker hypointense signals for nanocomplex-antiHER2 conjugates incubated with SKBR3 cells (Fig. 3c) relative to MDAMB231 cells (Fig. 3d). A merged fluorescence image of SKBR3 cells (Fig 3e) shows that the nanocomplexes bind specifically to receptors on the cell membrane. Since the MDAMB231 cell line has low HER2 expression, only a fraction of nanocomplex–anti-HER2 conjugates were bound, resulting in a much weaker near-infrared emission signal (Fig. 3f).

When illuminated with a 808 nm laser (200 mW, 3.72 Wcm^{-2}, 1 mm diameter spot size) nanocomplexes demonstrated high-efficacy photothermal ablation of SKBR3 cells. Nanocomplex–antiHER2 conjugates incubated with SKBR3 cells, when irradiated, produced hyperthermia specifically within the laser illuminated spot, resulting in cell death (Fig. 3g).. By comparison, fewer nanocomplex-antiHER2 conjugates were bound to MDAMB231 cells, resulting in fewer dead cells (Fig. 3h).

The theranostic potential of these nanocomplexes was demonstrated *in vivo* in breast cancer xenografts.[29] HER2-overexpressing human breast cancer cells, BT474AZ, and control, MDAMB231 cells were grown subcutaneously in a mouse model, and tumors were allowed to grow to 7–8 mm diameter. Nanocomplexes (200 μL, 9×10^9 particles/mL) were injected systemically into the mouse tail vein, and the animals were imaged postinjection. This dosage was analogous to ~5 μg of ICG/kg body weight, nearly 400X lower than the maximum FDA approved clinical dose of ICG. Near-infrared fluorescence images of mice with MDAMB231 xenografts and BT474AZ xenografts are shown at various postinjection time points (Fig. 4a). Fluorescence intensities of the tumors evaluated at different time points revealed a 71.5 % increase in the BT474AZ tumor intensity at 4 h compared to the intensity from MDAMB231 tumors. Within 72 h, most nanocomplexes appeared to be either cleared from the body or accumulated in the liver, indicated by the diminishing fluorescence intensity. Nanocomplex retention was also visualized with MRI. The T_2-weighted MR images of mice with MDAMB231 and BT474AZ xenografts imaged pre- and post-injection are shown (Fig. 4b). As nanocomplexes accumulate in the tumor, higher T_2 contrast is observed, resulting in a significantly darker appearance. Within 72 h, as nanocomplexes clear from the tumor, tumors regain their original appearance. Comparison of the MR intensities of tumors at different time points shows that BT474AZ tumors are ~50.5% darker at 24 hours compared to MDAMB231 tumors, with a maximum accumulation of the nanocomplex at 24 hours. Analogous to fluorescence imaging, MR images also show a higher accumulation of nanocomplexes in HER2-overexpressing tumors relative to the control.

The discrepancy observed between MRI and fluorescence imaging results is attributed, in part, to the lower sensitivity and signal-to-noise ratio of MRI. However, MRI offers high spatial resolution providing complete anatomical structural information of tumors relative to optical approaches. Fluorescence imaging offers exceptional sensitivity, however, due to the surface-weighted characteristics of this modality, nanocomplexes accumulated near the tumor surface are imaged preferentially. Nanocomplexes take longer to accumulate within the tumor core relative to the peripheral vasculature, contributing to the dissimilarity between the MRI and fluorescence analysis. Integrating these two complementary techniques within a single nanocomplex could be quite advantageous in establishing more accurate, ultimately quantitative, imaging methods.

The individual organs of the mice were analyzed to evaluate the biodistribution of the nanocomplexes at 72 hours postinjection. Near-infrared fluorescence images of tissues (Fig. 4c) retrieved from MDAMB231 and BT474AZ mice show maximum accumulation in the

tumor relative to other tissues. A surface averaged fluorescence intensity analysis, where fluorescence intensity was divided by the surface area of each tissue (Fig. 4d) correlate well with the images. The Au content in each tissue was also measured using inductively coupled plasma-mass spectrometry (ICP-MS), to independently verify, as quantitatively as possible, nanocomplex distribution in the tissues. The Au distribution (μg) per mass of tissue (g) for both BT474AZ and MDAMB231 mice (Fig. 4e) correlates well with the measured fluorescence intensities, albeit with some variations. In both tumor types, the tumors and liver have significant Au content. Since the liver is inherently highly absorbing at NIR wavelengths, nanocomplexes deeper in the liver may not be observable by fluorescence, but may be accurately measured by ICP-MS. These comparative studies illustrate the ability of nanocomplexes to target breast cancer cells, enhance images of the binding event and specific location on the cell surface, and deliver a therapeutic heating dose upon photothermal actuation.

Gene Therapy

Gene therapy is the process of inserting a small DNA or RNA sequence to modify the expression of certain specific proteins associated with disease. Two of the most promising gene therapies are antisense DNA and short interfering RNA (si-RNA) therapy. Both target messenger RNA (mRNA), the intermediary between the DNA and the protein, to selectively inhibit the expression of an unwanted protein (downregulation). In antisense therapy, short ss-DNA strands (15–30 bases) hybridize to the mRNA, blocking production of the disease-causing protein and activating the enzyme RNase H that degrades the mRNA. si-RNA therapy consists of delivering short ds-RNA sequences (19–21 bases) to the cells that first bind to RNA-induced silencing complex (RISC), an enzyme located within cells. This facilitates the binding of siRNA to mRNA, cleaving the mRNA and leading to downregulation of the undesired protein. While gene therapy holds tremendous promise in addressing a wide range of diseases, a major challenge is the delivery of oligonucleotide sequences into the cellular environment. Early experiments using viruses for gene delivery resulted in fatalities in clinical trials, greatly slowing the development of this approach.[39]

One of the most promising alternative technologies for gene delivery is the use of AuNPs as delivery vehicles.[40, 41] A variety of AuNPs of various shapes and sizes have been used in initial demonstrations of protein downregulation. AuNSs meet many of the desired characteristics for gene delivery: no immunogenic response, steric protection of bound DNA/RNA against nucleases, good cellular uptake and the facile gold surface chemistry.[30] The plasmonic properties of AuNSs that assist in the photothermal ablation of solid tumors maybe used to light-trigger the release of short DNA strands conjugated to the surface of AuNSs. The light triggered release of the DNA from AuNSs also allows precise temporal control over DNA/RNA release, potentially enabling a more detailed understanding of the kinetics of protein downregulation.

Light triggered release of antisense DNA from AuNSs was recently demonstrated.[30] The complementary strand to the antisense sequence was modified with a thiol moiety that allowed for facile conjugation of the sense strand to the AuNS surface (Fig. 5). The antisense strand (red) is hybridized to the thiolated complementary sense sequence (green), then attached to the Au to form a DNA monolayer on the AuNS surface. Gel electrophoresis was used to quantify the released ss-DNA in solution. A 3% agarose gel was used to separate the ss-DNA from the nanoshell-DNA complex.

Antisense DNA release from AuNSs by heating the solution conventionally, and by plasmon-resonant NIR light, was compared. DNA melting curves for a 20-base DNA oligonucleotide (TATGATCTGTCACAGCTTGA) released by heating the nanoshell-DNA

solution in a water bath (Fig. 5c) and by illuminating the solution with a NIR laser (Fig. 5d) are shown. The maximum of the first derivative of the melting profile corresponds to the melting temperature (Tc) at which 50% of the DNA is released. For the antisense oligonucleotide used, the release temperature was found to be 37 °C, while for NIR light release, Tc occurred at a solution ambient temperature of 27 °C. Several oligomers of varying length and composition were studied. Similar dramatic lowering of the DNA melting temperature for the resonant light-induced release was observed consistently for various lengths and compositions of DNA (Fig. 5b).[30] DNA release always occurred prior to any significant heating of the AuNS solution: this is an essential regime for biological applications, ensuring that DNA can be released using light without the induction of hyperthermic cell death.[42] The coverage was determined to be 6400 ds-DNA/nanoshell, corresponding to a concentration of 14.6 pmol/cm^2. In the two experiments[30] ~ 90% of the ss-DNA was released in the thermal release experiment while ~ 50% was released using light at near-ambient temperature.

In addition to the release of antisense DNA, the ds-DNA-AuNS complex serves as an effective host for the directed delivery of other small molecules into cells. Molecules may associate with ds-DNA by intercalating between the grooves of the ds-DNA.[43] The light triggered release of the antisense-DNA and delivery of small molecules into cells has been recently demonstrated using DAPI molecules with ds-DNA bound to AuNSs. DAPI is a watersoluble blue fluorescent dye that binds reversibly in the minor groove of ds-DNA and is frequently used to stain cells to visualize their nuclei.

ds-DNA-nanoshell complexes were loaded with DAPI by incubating DAPI solution with ds-DNA-nanoshell complexes, then incubated with H1299 lung cancer cells to allow uptake of the complexes.[31] Upon illumination with an 800 nm CW laser (1W/cm^2, 5 min), corresponding to the peak resonant wavelength of the AuNS complexes, the ds-DNA dehybridizes and the ss-DNA and the DAPI molecules are released within the cells. Subsequent to release, the DAPI diffuses through the cytoplasm and into the cell nucleus, where it preferentially binds to and stains the nuclear DNA.

To quantify the fluorescence of the DAPI bound to just the nuclear DNA without measuring the fluorescence from the cytoplasm of the cell, the cell nuclei were isolated and the DAPI fluorescence of the nuclei were measured by flow cytometry. The normalized histograms of DAPI fluorescence intensity versus number of nuclei from H1299 cells incubated with ds-DNA-AuNS-DAPI before and after laser treatment are shown (Fig. 6a). After laser treatment, the fluorescence intensity of the nuclei increased significantly. A ~33% increase in fluorescence intensity is observed. Epifluorescence images of H1299 cells incubated with AuNS-dsDNA-DAPI before (Figure 6c, left) and after (Figure 6c, right) laser treatment clearly show a marked increase in DAPI fluorescence. A control experiment consisting of H1299 cells incubated with DAPI only (no AuNSs) was conducted (Figure 6b). The cells were irradiated with the NIR laser under conditions identical to the previous experiment. The mean DAPI fluorescence intensity did not significantly increase after laser irradiation. Many classes of molecules can intercalate into ds-DNA, including antibiotics, steroids, and chemotherapeutic molecules, making this ds-DNA-AuNS platform an extremely promising and highly general controlled intracellular delivery mechanism.

Summary and Future Perspectives

This account summarizes the progress of nanoshells from standalone photothermal actuators to multifunctional theranostic nanocomplexes with targeting, contrast enhancement for diagnostics, photothermal therapy and gene therapy capabilities. Since nanoshell-based photothermal therapy has already transitioned to clinical trials, we envision the theranostic

possibilities of nanoshells will also see significant progress within the next decade for applications *in vitro*, *in vivo* and in adjuvant settings.[44] Theranostic nanoparticles as delivery vectors should ultimately allow us to simultaneously visualize and deliver therapeutics to metastatic cancer sites.[23] The mortality rate of patients with macroscopic metastatic disease continues to be significantly high due to acquired resistance. Furthermore, theranostic nanoparticles which combine multiple imaging modalities may ultimately enable us to monitor processes, therapeutic mechanisms and outcomes in disease sites which have remained largely inaccessible, for example, the brain.

Theranostics is truly emblematic of the evolution of multidisciplinary nanoscience, as a gradual convergence of multiple disciplines including chemistry, material science, electromagnetics, biology, medical physics and oncology. We can predict high-impact advances in this field as researchers' pioneer approaches to develop nanoscale platforms with multiple functionalities. However, several aspects must be evaluated before theranostics can advance, including nanoparticle size and surface characteristics, appropriate dosage of both diagnostic and therapeutic functions, toxicity and biocompatibility as controlled by the surface chemistry of the nanocomplexes, the detailed tracking of theranostic nanoparticles and their interactions *in vivo*. Pursuing these important aspects will enable theranostics to transition from laboratory to clinical settings.

Acknowledgments

This work was support by the Department of Defense NSSEFF, the Air Force Office of Scientific Research (FA9550-10-1-0469) and the Robert A. Welch Foundation (C-1220) (R.B., S.L. and N.J.H.). A.J. was supported by Baylor College of Medicine Faculty seed grant No. 2680150801, Caroline M Weiss Junior Faculty seed award, and NIH grants R42-CA115028, R01-CA151962 and U01 CA 151886.

Biographies

Rizia Bardhan received her Ph.D. in Chemistry in 2010 from Rice University under the supervision of Prof. Halas. Her research focused on the design of multimodal nanoparticles for imaging and therapy. She is currently pursuing postdoctoral research at Lawrence Berkeley National Laboratory.

Surbhi Lal received her Ph.D. in Applied Physics from Rice University. She has been a research associate with Prof. Halas at Rice University since 2006. Her research interests include surface enhanced spectroscopy, plasmonics and nanophotonics.

Prof. Amit Joshi is Assistant Professor of Radiology at Baylor College of Medicine. His current research interests are fluorescence optical tomography, molecular imaging and application of nanoparticles for imaging and cancer therapy.

Prof. Naomi Halas is the Stanley C. Moore Professor in Electrical and Computer Engineering, Professor of Chemistry, Bioengineering, and Physics at Rice University. She is the inventor of nanoshells and has demonstrated numerous applications for nanoshells in biomedicine and biochemical sensing. She is author of over 200 publications, has over 10 issued patents, and over 350 invited talks. She was elected to the American Academy of Arts and Sciences in 2009.

REFERENCES

1. ACS, Cancer Facts & Figures. American Cancer Society. 2010.
2. Grobner T, Prischl FC. Gadolinium and nephrogenic systemic fibrosis. Kidney Inter. 2007; 72:260–264.

3. Wang J, Short D, Sebire NJ, Lindsay I, Newlands ES, Schmid P, Savage PM, Seckl MJ. Salvage Chemotherapy of Relapsed or High-risk Gestational Trophoblastic Neoplasia (GTN) with Paclitaxel/cisplatin Alternating with Paclitaxel/etoposide (TP/TE). Ann. Oncol. 2008; 19:1578–1583. [PubMed: 18453518]
4. Davis ME, Chen ZG, Shin DM. Nanoparticle therapeutics: an emerging treatment modality for cancer. Nat. Rev. Drug Discovery. 2008; 7:771–782.
5. Peer D, Karp JM, Hong S, Farokhzad OC, Margalit R, Langer R. Nanocarriers as an emerging platform for cancer therapy. Nat. Nanotech. 2007; 2:751–760.
6. Brannon-Peppas L, Blanchette JO. Nanoparticle and Targeted Systems for Cancer Therapy. Adv. Drug Deliver. Rev. 2004; 56:1649–1659.
7. Park K, Lee S, Kang E, Kim K, Choi K, Kwon IC. New Generation of Multifunctional Nanoparticles for Cancer Imaging and Therapy. Adv. Func. Mater. 2009; 19:1553–1566.
8. Weissleder R, Pittet MJ. Imaging in the Era of Molecular Oncology. Nature. 2008; 452:580–589. [PubMed: 18385732]
9. Boisselier E, Astruc D. Gold Nanoparticles in Nanomedicine: Preparations, Imaging, Diagnostics, Therapies and Toxicity. Chem. Soc. Rev. 2009; 38:1759–1782. [PubMed: 19587967]
10. Bartlett DW, Su H, Hildebrandt IJ, Weber WA, Davis ME. Impact of Tumor-Specific Targeting on the Biodistribution and Efficacy of SiRNA Nanoparticles Measured by Multimodality *in Vivo* Imaging. Proc. Natl. Acad. Sci. USA. 2007; 104:15549–15554. [PubMed: 17875985]
11. Huang X, El-Sayed IH, Qian W, El-Sayed MA. Cancer Cell Imaging and Photothermal Therapy in the Near-Infrared Region by Using Gold Nanorods. J. Am. Chem. Soc. 2006; 128:2115–2120. [PubMed: 16464114]
12. Kim D, Jeong YY, Jon S. A Drug-Loaded Aptamer-Gold Nanoparticle Bioconjugate for Combined CT Imaging and Therapy of Prostate Cancer. ACS Nano. 2010; 4:3689–3696. [PubMed: 20550178]
13. Kim J-W, Galanzha EI, Shashkov EV, Moon H-M, Zharov VP. Golden Carbon Nanotubes as Multimodal Photoacoustic and Photothermal High-contrast Molecular Agents. Nat. Nanotech. 2009; 4:688–694.
14. McCarthy JR, Jaffer FA, Weissleder R. A Macrophage-Targeted Theranostic Nanoparticle for Biomedical Applications. Small. 2006; 2:983–987. [PubMed: 17193154]
15. Nasongkla N, Bey E, Ren J, Ai H, Khemtong C, Guthi JS, Chin S-F, Sherry AD, Boothman DA, Gao J. Multifunctional Polymeric Micelles as Cancer-Targeted, MRI-Ultrasensitive Drug Delivery Systems. Nano Letters. 2006; 6:2427–2430. [PubMed: 17090068]
16. Rapoport N, Gao Z, Kennedy A. Multifunctional Nanoparticles for Combining Ultrasonic Tumor Imaging and Targeted Chemotherapy. J Natl Cancer Inst. 2007; 99:1095–1106. [PubMed: 17623798]
17. Santra S, Kaittanis C, Grimm J, Perez JM. Drug/Dye-Loaded, Multifunctional Iron Oxide Nanoparticles for Combined Targeted Cancer Therapy and Dual Optical/Magnetic Resonance Imaging. Small. 2009; 5:1862–1868. [PubMed: 19384879]
18. McCarthy JR. The Future of Theranostic Nanoagents. Nanomedicine. 2009; 4:693–695. [PubMed: 19839803]
19. Sumer B, Gao JM. Theranostic Nanomedicine for Cancer. Nanomedicine. 2008; 3:137–140. [PubMed: 18373419]
20. Daniel M-C, Astruc D. Gold Nanoparticles: Assembly, Supramolecular Chemistry, Quantum-Size-Related Properties, and Applications toward Biology, Catalysis, and Nanotechnology. Chem. Rev. 2004; 104:293–346. [PubMed: 14719978]
21. Lal S, Clare SE, Halas NJ. Nanoshell-Enabled Photothermal Cancer Therapy: Impending Clinical Impact. Acc. Chem. Res. 2008; 41:1842–1851. [PubMed: 19053240]
22. Brinson BE, Lassiter JB, Levin CS, Bardhan R, Mirin N, Halas NJ. Nanoshells Made Easy: Improving Au Layer Growth on Nanoparticle Surfaces. Langmuir. 2008; 24:14166–14177. [PubMed: 19360963]
23. Choi M-R, Stanton-Maxey KJ, Stanley JK, Levin CS, Bardhan R, Akin D, Badve S, Sturgis J, Robinson JP, Bashir R, Halas NJ, Clare SE. A Cellular Trojan Horse for Delivery of Therapeutic Nanoparticles into Tumors. Nano Letters. 2007; 7:3759–3765. [PubMed: 17979310]

24. Gobin AM, Lee MH, Halas NJ, James WD, Drezek RA, West JL. Near-Infrared Resonant Nanoshells for Combined Optical Imaging and Photothermal Cancer Therapy. Nano Letters. 2007; 7:1929–1934. [PubMed: 17550297]
25. Bardhan R, Grady NK, Cole J, Joshi A, Halas NJ. Fluorescence Enhancement by Au nanostructures: nanoshells and nanorods. ACS Nano. 2009; 3:744–752. [PubMed: 19231823]
26. Bardhan R, Grady NK, Halas NJ. Nanoscale Control of Near-Infrared Fluorescence Enhancement using Au Nanoshells. Small. 2008; 4:1716–1722. [PubMed: 18819167]
27. Bardhan R, Chen W, Perez-Torres C, Bartels M, Huschka RM, Zhao LL, Morosan E, Pautler RG, Joshi A, Halas NJ. Nanoshells with Targeted Simultaneous Enhancement of Magnetic and Optical Imaging and Photothermal Therapeutic Response. Adv. Func. Mater. 2009; 19:3901–3909.
28. Chen W, Bardhan R, Bartels M, Perez-Torres C, Pautler RG, Halas NJ, Joshi A. A Molecularly Targeted Theranostic Probe for Ovarian Cancer. Mol. Cancer Therapeutics. 2010; 9:1028–1038.
29. Bardhan R, Chen W, Bartels M, Perez-Torres C, Botero MF, McAninch RW, Contreras A, Schiff R, Pautler RG, Halas NJ, Joshi A. Tracking of Multimodal Therapeutic Nanocomplexes Targeting Breast Cancer *in vivo*. Nano Letters. 2010; 10:4920–4928.
30. Barhoumi A, Huschka R, Bardhan R, Knight MW, Halas NJ. Light-induced Release of DNA from Plasmon-resonant Nanoparticles: Towards Light-controlled Gene Therapy. Chem. Phys. Lett. 2009; 482:171–179.
31. Huschka R, Neumann O, Barhoumi A, Halas NJ. Visualizing Light-Triggered Release of Molecules Inside Living Cells. Nano Letters. 2010; 10:4117–4122. [PubMed: 20857946]
32. Loo C, Lin A, Hirsch LR, Lee MH, Barton J, Halas NJ, West JL, Drezek R. Nanoshell-enabled photonics-based imaging and therapy of cancer. Technol. Cancer Res. Treat. 2004; 3:33–40. [PubMed: 14750891]
33. Link S, El-Sayed MA. Optical Properties and Ultrafast Dynamics of Metallic Nanocrystals. Annu. Rev. Phys. Chem. 2003; 54:331–336. [PubMed: 12626731]
34. Drexhage KH. Influence of a Dielectric Interface On Fluorescence Decay Time. J. Lumin. 1970; 1:693–701.
35. Waldeck DH, Alivisatos AP, Harris CB. Nonradiative Damping of Molecular Electronic Excited States by Metal Surfaces. Surf. Sci. 1985; 158:103–125.
36. Hirsch LR, Stafford RJ, Bankson JA, Sershen SR, Rivera B, Price RE, Hazle JD, Halas NJ, West JL. Nanoshell-mediated near-infrared thermal therapy of tumors under magnetic resonance guidance. Proc. Natl. Acad. Sci. USA. 2003; 100:13549–13554. [PubMed: 14597719]
37. Loo C, Lowery A, Halas NJ, West JL, Drezek RA. Immunotargeted Nanoshells for Integrated Cancer Imaging and Therapy. Nano Letters. 2005; 5:709–711. [PubMed: 15826113]
38. Wang Y, Xie X, Wang X, Ku G, Gill KL, O'Neal DP, Stoica G, Wang LV. Photoacoustic Tomography of a Nanoshell Contrast Agent in the in Vivo Rat Brain. Nano Letters. 2004; 4:1689–1692.
39. Israel ZH, Domb AJ. Polymers in Gene Therapy: Antisense Delivery Systems. Polym. Adv. Technol. 1998; 9:799–805.
40. Seferos DS, Prigodich AE, Giljohann DA, Patel PC, Mirkin CA. Polyvalent DNA Nanoparticle Conjugates Stabilize Nucleic Acids. Nano Lett. 2009; 1:308–311. [PubMed: 19099465]
41. Giljohann DA, Seferos DS, Prigodich AE, Patel PC, Mirkin CA. Gene Regulation with Polyvalent siRNA-Nanoparticle Conjugates. J. Am. Chem. Soc. 2009; 131:2072–2073. [PubMed: 19170493]
42. Demers LM, Mirkin CA, Mucic RC, Reynolds RA, Letsinger RL, Elghanian R, Viswanadham G. A Fluorescence-Based Method for Determining the Surface Coverage and Hybridization Efficiency of Thiol-Capped Oligonucleotides Bound to Gold Thin Films and Nanoparticles. Anal. Chem. 2000; 72:5535–5541. [PubMed: 11101228]
43. Neto BAD, Lapis AAM. Recent Developments in the Chemistry of Deoxyribonucleic Acid (DNA) Intercalators: Principles, Design, Synthesis, Applications and Trends. Molecules. 2009; 14:1725–1746. [PubMed: 19471193]
44. Diagaradjane P, Shetty A, Wang JC, Elliott AM, Schwartz J, Shentu S, Park HC, Deorukhkar A, Stafford RJ, Cho SH, Tunnell JW, Hazle JD, Krishnan S. Modulation of in Vivo Tumor Radiation Response via Gold Nanoshell-Mediated Vascular-Focused Hyperthermia: Characterizing an

Integrated Antihypoxic and Localized Vascular Disrupting Targeting Strategy. Nano Lett. 2008; 8:1492–1500. [PubMed: 18412402]

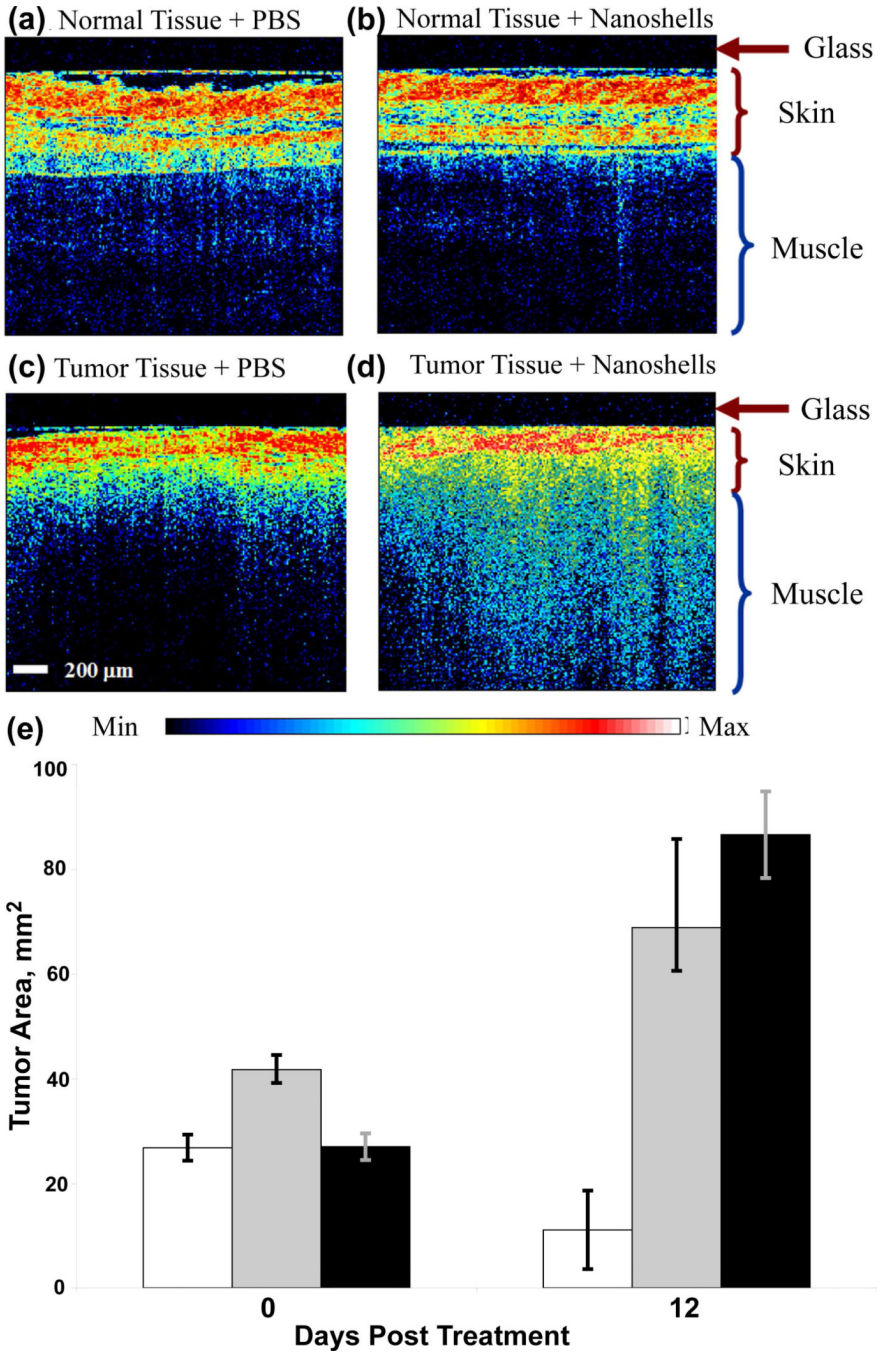

FIGURE 1.

OCT images of normal tissue of mice systemically injected with (a) PBS and (b) nanoshells and tumor tissue injected with (c) PBS and (d) nanoshells. The dark nonscattering layer is 200 µm thick glass of the probe. (e) Tumor size before irradiation and 12 days post-irradiation with near-infrared laser of mice treated with nanoshells (white), PBS (gray) and untreated control (black). Reproduced with permission from ref.24.

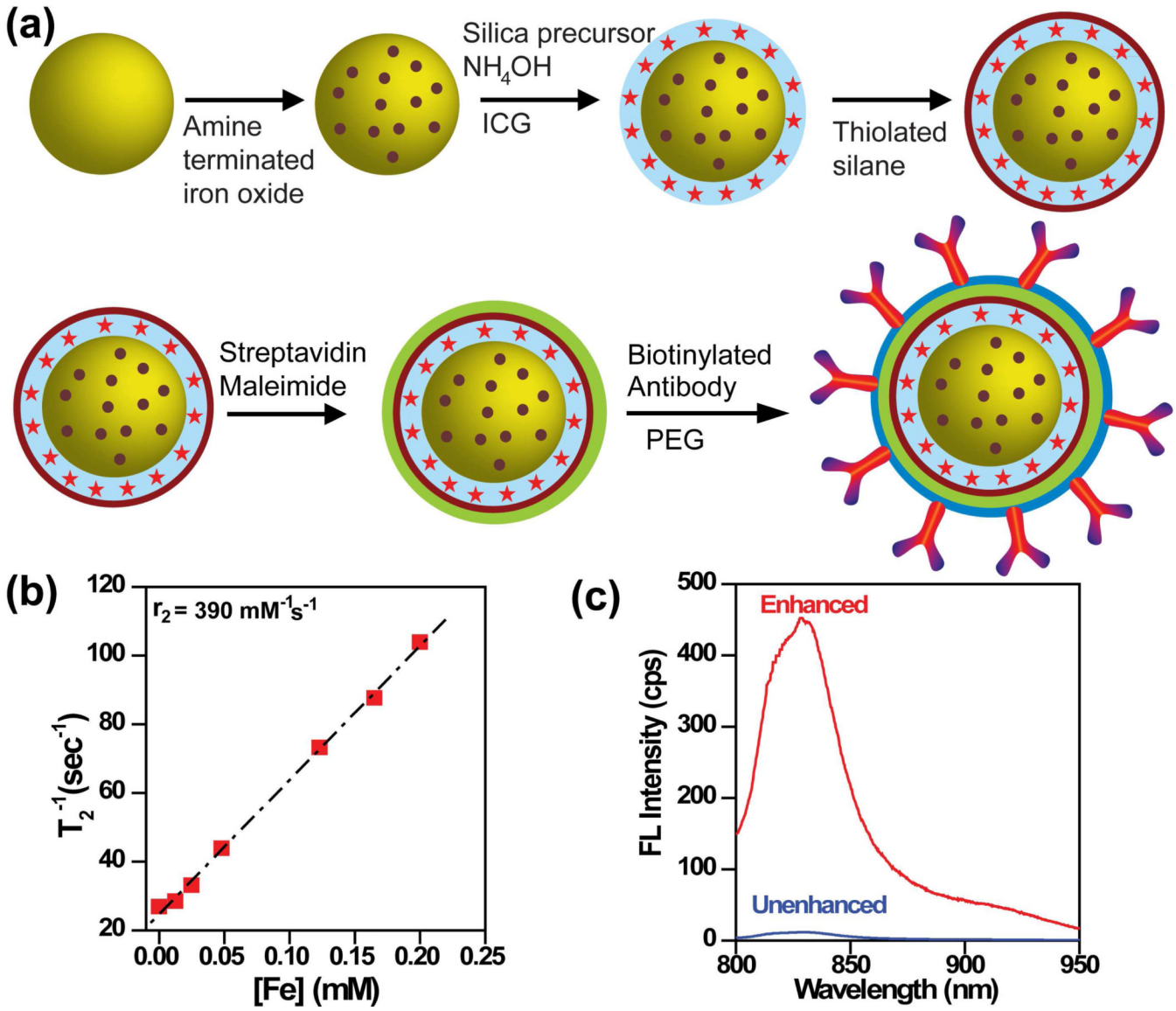

FIGURE 2.

(a) Illustration of nanocomplexes fabrication and conjugation to antibodies. (b) Spin–spin relaxation rate (T_2^{-1}) as a function of [Fe] of the nanocomplexes. r_2 is relaxivity obtained from the slope. (c) Fluorescence (FL) spectra of enhanced ICG doped within silica layer of nanocomplexes, and unenhanced control, ICG doped within silica nanospheres. Reproduced with permission from ref.27.

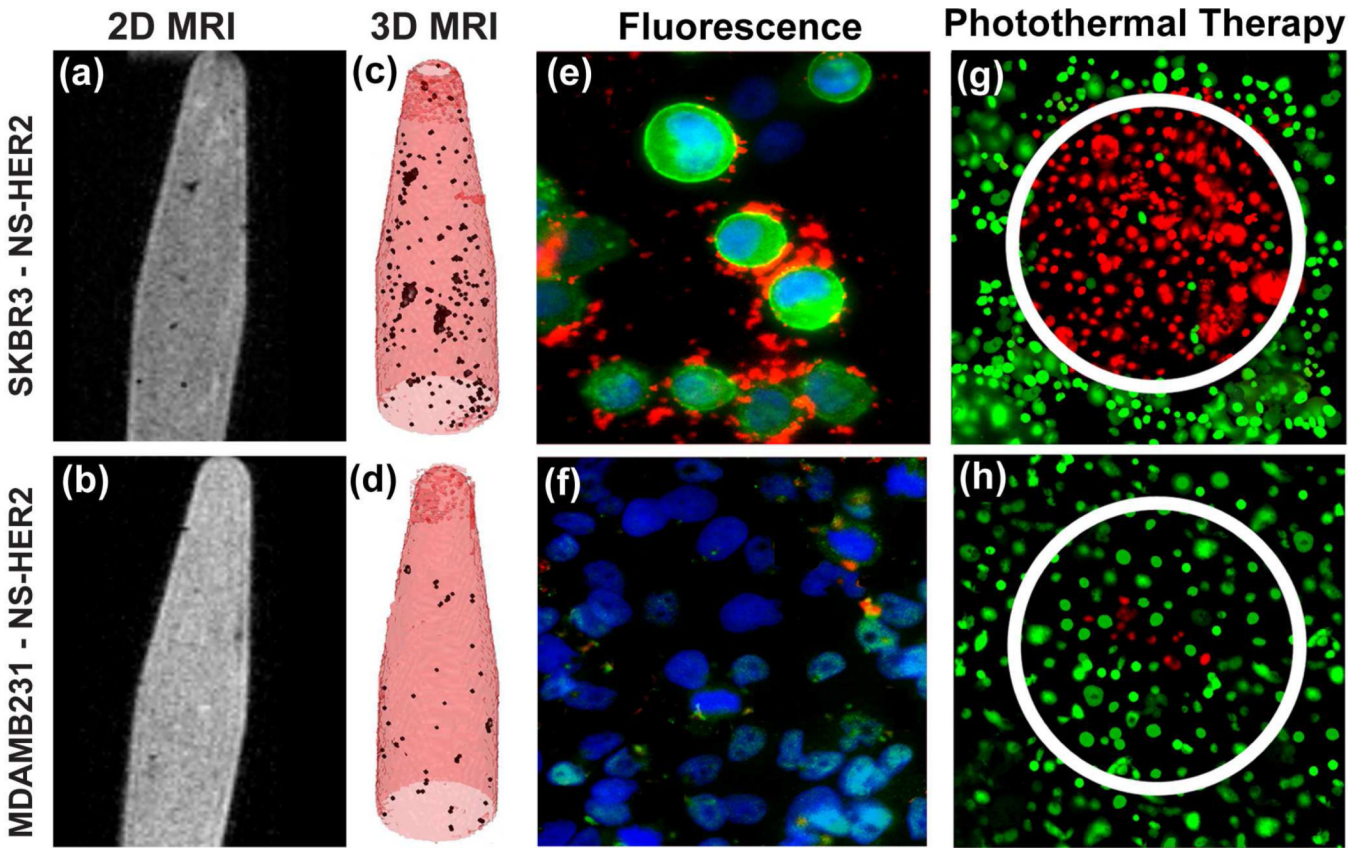

FIGURE 3.

Images of SKBR3 cells (top) and control, MDAMB231 cells (bottom), incubated with nanocomplex–anti-HER2 conjugates. (a, b) MR images of nanocomplexes bound to cells suspended in agarose. (c, d) Maximum intensity projection of T_2 maps of the images corresponding to (a) and (b) respectively. Fluorescence images of (e) SKBR3 cells showing nanocomplexes binding on cell surface, (f) MDAMB231 cells showing some nonspecific binding (g, h) Photothermal ablation of cells incubated with nanocomplex–anti-HER2 and treated with NIR laser at 808 nm. Live cells are stained green with calcein and dead cells are stained red with PI. Reproduced with permission from ref.27.

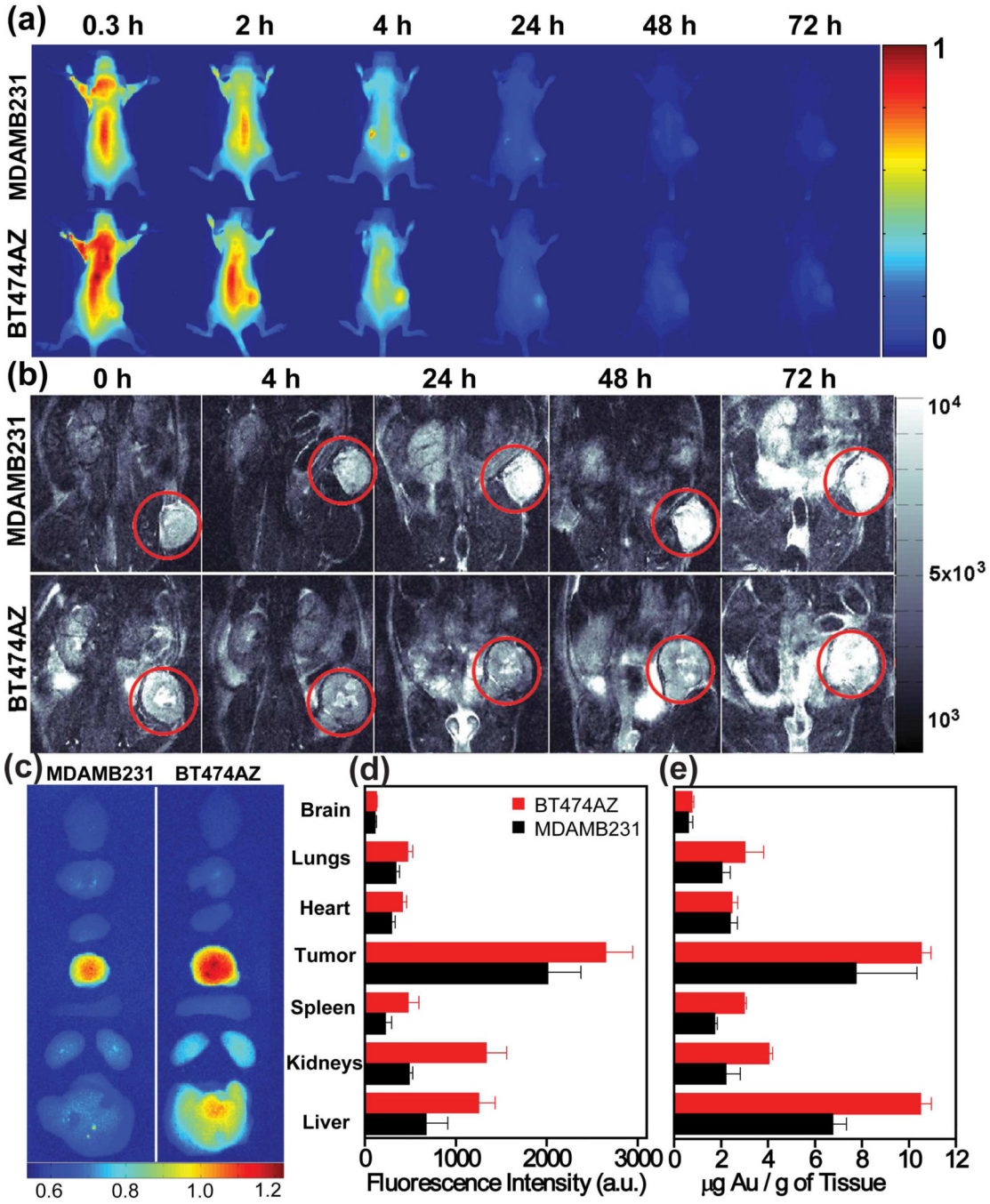

FIGURE 4.

Nanocomplexes delivery *in vivo* observed with near-infrared fluorescence imaging of mice with (a) control, MDAMB231 xenografts (top) and BT474AZ xenografts (bottom) at 0.3–72 h post-injection of nanocomplexes. T_2-weighted MRI images of (b) MDAMB231 xenografts (top) and BT474AZ xenografts (bottom) pre-injection 0 h, and 4–72 h post-injection of nanocomplexes. Tumor is marked with red circle. (c) Near-infrared fluorescence images of mice tissues harvested from BT474AZ (left) and MDAMB231 (right) 72 h post-injection of nanocomplexes. (d) Fluorescence intensity analysis of mice organs of BT474AZ (red) and MDAMB231 (black). (e) Gold distribution (from ICP-MS) in mice tissue. Reproduced with permission from ref.29.

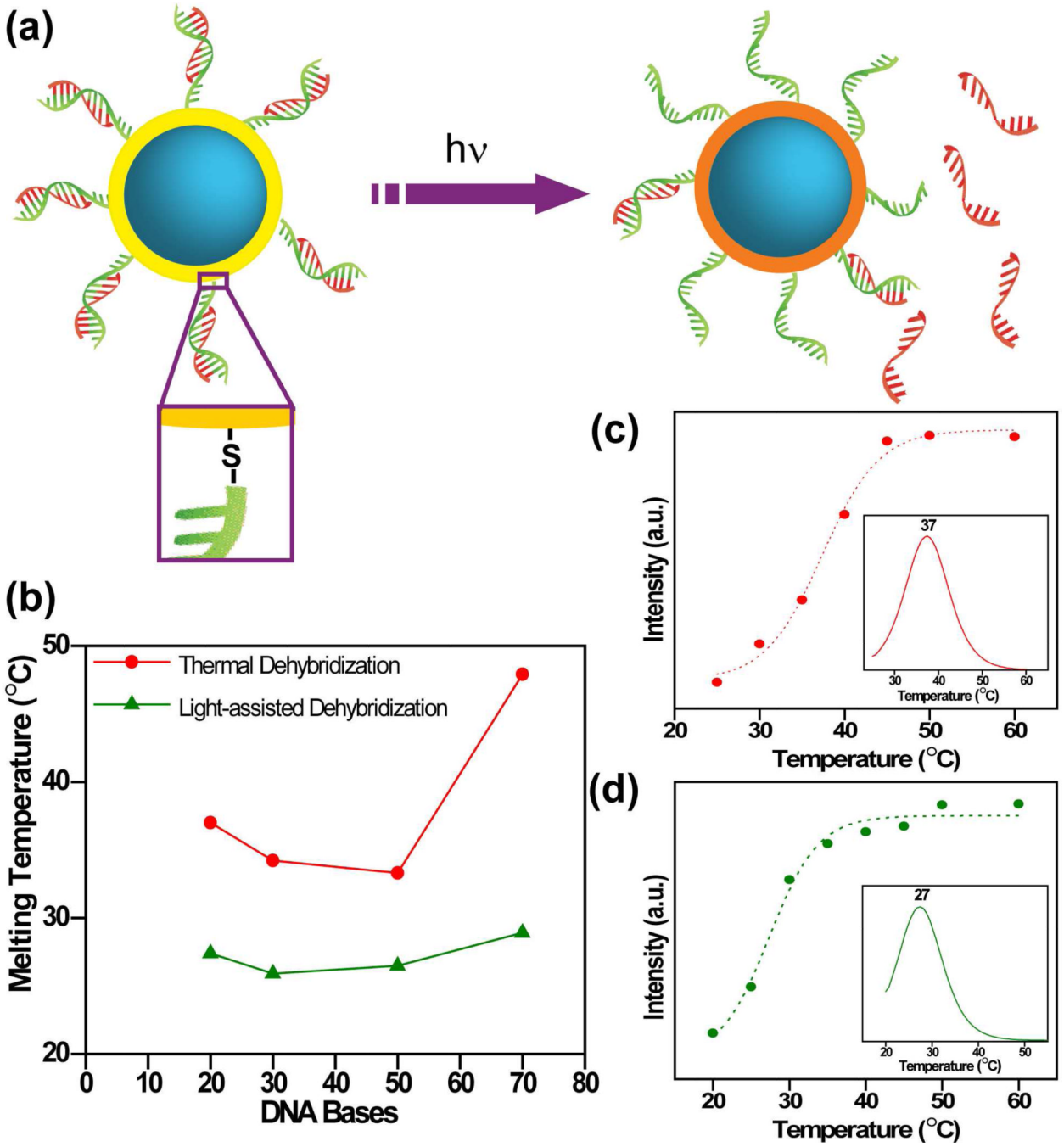

FIGURE 5.

(a) Schematic of light-controlled release of ssDNA from nanoshells when illuminated with resonant near-infrared light. Thiolated sense sequences (green) are bound to nanoshell surface and antisense sequences (red) are released. (b) Comparison of light-induced (green) versus thermal (red) dehybridization of dsDNA sequences of different lengths tethered to nanoshells. (c) Thermal and (d) light-induced release of ssDNA from dsDNA-coated nanoshells in solution. Melting curves for 20 base dsDNA attached to nanoshell surface are shown. Insets show first derivatives of the melting curves, depicting melting temperatures of each process. Reproduced with permission from ref.30.

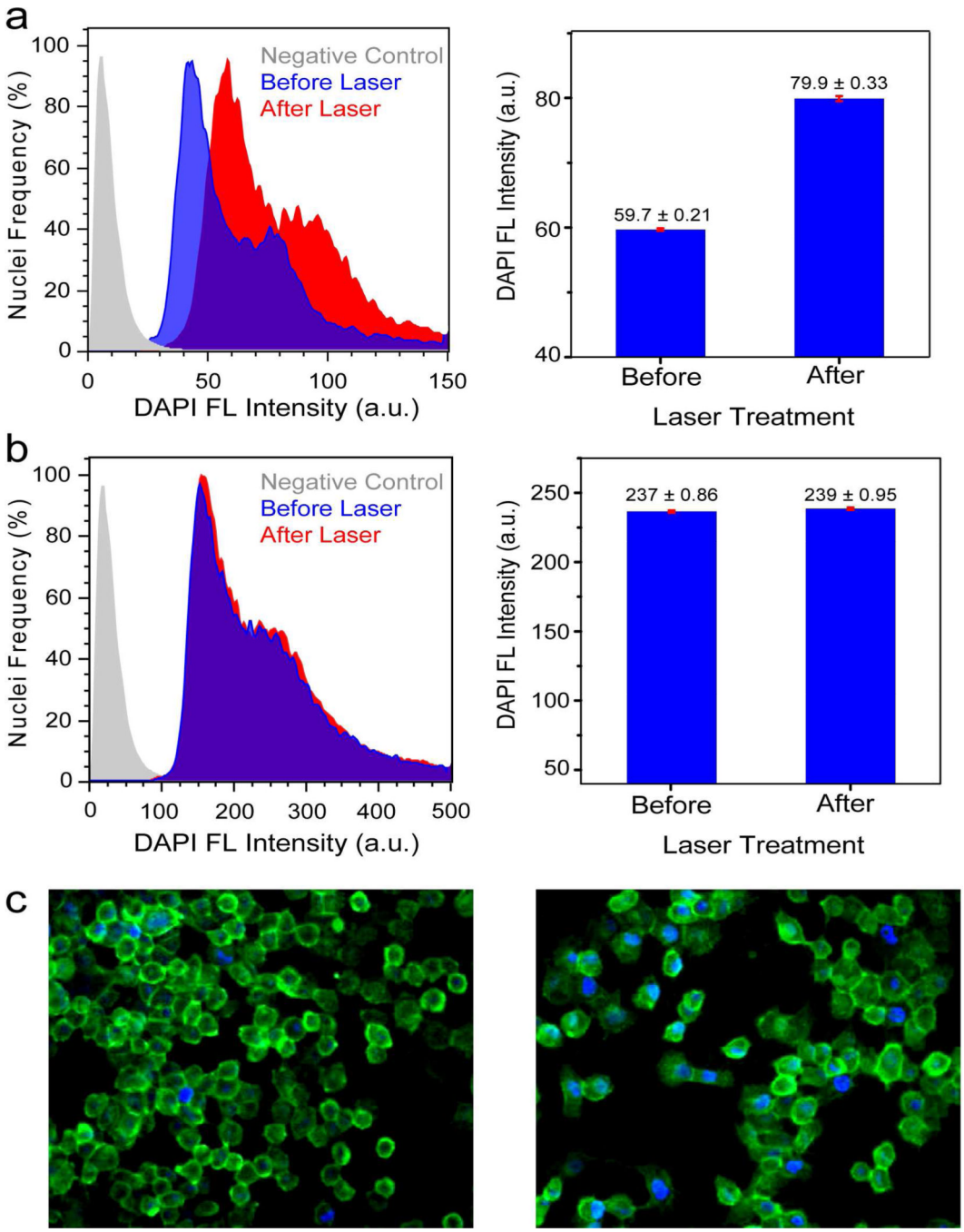

FIGURE 6.

Flow cytometry histograms of DAPI Fluorescence versus number of isolated nuclei from H1299 cells incubated with (a) nanoshell-dsDNA-DAPI and (b) DAPI (control). Control (gray), treated cells without laser irradiation (blue) and treated cells with laser irradiation (red). Bar graphs display the mean DAPI fluorescence intensity±SEM before and after laser irradiation. (c) Epifluorescence images of H1299 cells incubated with nanoshell-dsDNA-DAPI (left) before and (right) after laser treatment. The cell membrane is marked by Alexa-Fluor488 (green). Reproduced with permission from ref.31.

TABLE 1

Imaging and therapeutic capabilities of nanoparticles

	Modality	**Nanoparticle / Agent**
Imaging	Optical scattering / OCT	Gold nanoshells, nanorods, nanocages, nanoparticles
	Fluorescence	Quantum dots, dye-doped silica, carbon nanotubes, organic fluorophores, phosphors
	MRI	Manganese-based, Iron oxide, Gadolinium agents, Perfluorocarbon
	PET, SPECT	Radioisotopes(^{64}Cu, ^{18}F, ^{124}I, ^{11}In)
	CT	Gold nanoparticles, Iodine
	Ultrasound	Polymeric nanoparticles, perfluropentane
Therapeutic Actuation	Photothermal	Gold nanoshells, nanorods, nanocages, nanoparticles
	Brychatherapy	^{198}Au,^{125}I, ^{103}Pd (X-rays)
	Photoacoustic	Carbon nanotubes
	Chemotherapy	Anticancer drugs (doxorubicin, paclitaxel etc.)
	Photodynamic	Photosensitizer
	Gene Therapy	siRNA, DNA
	Magnetic hyperthermia	Iron oxide based nanoparticles
	Radiotherapy	^{64}Cu radionucleotide
	Neutron capture therapy	Gadolinium, Boron

OCT: optical coherence tomography, MRI: magnetic resonance imaging, PET: positron emission tomography, SPECT: single photon emission computed tomography, CT: computed tomography